Colloids and Surfaces B: Biointerfaces 84 (2011) 35–43

Contents lists available at ScienceDirect

Colloids and Surfaces B: Biointerfaces

journal homepage: www.elsevier.com/locate/colsurfb

Cell adhesion and locomotion on microwell-structured glass substrates

Yanbin Guan, William Kisaalita*

Cellular Bioengineering Laboratory, Faculty of Engineering and Biological and Agricultural Engineering Department, University of Georgia, Athens, GA 30602, USA

ARTICLE INFO

Article history:
Received 19 July 2010
Received in revised form
30 November 2010
Accepted 2 December 2010
Available online 9 December 2010

Keywords:
Laser ablation
Cell adhesion
Cell locomotion
Time-lapse microscopy
Image processing

ABSTRACT

The purpose of this study was to investigate the effect of microstructured material surface on cell adhesion and locomotion in real-time. ArF excimer laser direct-writing ablation was used to fabricate microwell patterns with precise control of size and spacing on glass. The influence of the ablation process parameters (laser fluence, pulse number and repetition rate) on the micromachining quality (depth, width, aspect ratio and edge effects) of the microwells was established. Human fibroblast cells, as an example of anchorage-dependent cells, were seeded onto the microstructured glass substrate and time-lapse microscopy was used to study cell adhesion and locomotion. The interaction with microstructured materials resulted in fibroblast cell repulsion and the cells exhibited a higher locomotion speed (75.77 ± 3.36 μm/h) on the structures in comparison with plane glass control (54.01 ± 15.53 μm/h). Further studies are needed to firmly establish the potential of microstructuring, for example, in elongating the life spans of implantable devices.

1. Introduction

The deleterious effect that biofouling has on biosensor stability is a serious impediment to the development of long-term implantable biosensors and largely accounts for the failure of in vivo biosensors [1]. Biofouling occurs as soon as a foreign item is implanted into the human body. Proteins, cells and other biological materials can deposit and accumulate on the sensor surface, which initiates the development of a bio-layer and scar-like capsule, leading to reduced analyte diffusion and perfusion to implanted sensors which ultimately causes a rapid decrease in sensor response. To explore anti-biofouling possibilities, immense interest has been paid to investigate the interaction between biomaterial surfaces and living cells as the first step [2,3]. The ability of cells to interact with the exposed material surface can affect the success of implanted medical devices (orthopedic implants, cardiovascular prosthesis and neural electrodes, etc.). The size, shape, alignment, and orientation of cells are greatly influenced by their local environment, the topography, and composition of the extra-cellular matrix (ECM) can significantly affect cellular functions, such as adhesion, growth, motility, secretion, gene expression, and apoptosis [4]. In contrast with chemical modifications that can degrade over time when exposed to harsh in vivo environment, surface topographical properties are generally much more stable.

Numerous studies have been conducted in directing cell adhesion and locomotion by controlling the material topology [5,6] and cells have been found to respond differently to smooth surfaces compared to materials with micro- or nano-scale features in a cell-type-dependent manner [7,8]. However, conflicting results were reported on the effect of microstructure on cell adhesion. Cell adhesion [9] and proliferation [10] were promoted, in the presence of microtexture on polymer substrates but were reduced in Campbell and Von's work [11]. To better understand the relationship between topography and cell fate, it is necessary to carry out dynamic observation after cell seeding in order to examine the initial cell responses to the microstructure. To date, little work has been done [12] on the effect of size, shape and aspect ratio of synthetic micro-structured surfaces on cell adhesion and locomotion in real-time.

The ever growing need and interest in the precise fabrication of microstructures call for new techniques that are capable of producing high-resolution structures, preferably in a high throughput manner. Photolithography is widely used, but the process requires use of a clean room, which may be an expensive investment. Electro-discharge machining (EDM) is a more direct micro-machining technique; however, it is only suitable for conductive materials. Laser, on the other hand, has undergone rapid development and has been applied to fine machining problems in diverse fields [13]. Laser micro-machining can process a variety of materials, glass, silicon, metals, inorganic, plastics, etc., both conductive and non-conductive, without a vacuum chamber or access to a clean room [14,15].

We chose laser micro-machining for microstructuring in this study for three reasons: First, laser beams exhibit low divergence, providing high precision and repeatability that fit into many special applications. Additionally, laser techniques offer

* Corresponding author. Tel.: +1 706 542 0835; fax: +1 706 542 8806.
E-mail address: williamk@engr.uga.edu (W. Kisaalita).

0927-7765/$ – see front matter © 2010 Elsevier B.V. All rights reserved.
doi:10.1016/j.colsurfb.2010.12.007

more exact temporal and spatial characteristics as they generate short pulses of monochromatic (single-wavelength) light. This light under precise control, directs high-density photon energy onto a selected local region of substrate material, resulting in minimal heat-affected zone especially when UV laser wavelength with high photon energy is used. Second, the non-contact process of direct laser irradiation not only introduces no tool wear as opposed to traditional micro-machines or EDM, but also minimizes the chance of damage to material due to process shock or handling. Laser micro-machining provides an easy one-step alternative to conventional chemical etching process without involving any solvent chemicals. Third, laser processing systems, incorporated with advanced computer control with user-friendly programming interfaces, permit easy retooling to fabricate flexible feature size and shape [16]. The main disadvantage of laser micromachining is debris formation. Other disadvantages include relatively high cost and it is time-consuming due to serial machining process.

Glass was chosen in this study mainly in view of its optical properties that enable microscopic observation. Other desirable properties include chemical inertness and proven long-term biocompatibility. Glass, on which the first microfluidic devices were fabricated by photolithography [17], is a common material convenient to use at low cost for biological studies. When glass is treated with serum-containing medium, a protein film form and facilitates cell adhesion [18]. In this study, gelatin coating was adopted to further enhance protein adsorption for cell adhesion onto glass substrates. Coating with gelatin should render extending the results to polymers or other materials coated with the same protein. Numerous reports have utilized polymers for applications in micro-fluidics or micro-/nano-biology [19], as polymers can be functionalized by various means [20].

We have interfaced human fibroblasts with high-aspect-ratio microwells, fabricated on glass by laser ablation, and observed the cell-material interaction using time-lapse microscopy in the initial hours of seeding. Direct observation of cell adhesion, spreading and locomotion on different microstructured (different microwell sizes) surfaces has revealed that cells avoid laser-ablated microwells, suggesting potential for anti-biofouling applications of microstructured surfaces.

2. Materials and methods

2.1. Glass micromachining and characterization

The computer-controlled laser system used in this study consisted of a workstation (Rapid X250 from Resonetics, NH), an excimer laser (ATLEX 500SI from ATL, Wermelskirchen, Germany) coupled to argon fluoride (ArF) gas (Spectra Gases, NJ). All experiments were carried out using ArF laser with a 193 nm wavelength at room temperature. ArF was chosen as opposed to KrF due to its shorter optical wavelength which causes less thermal effects and permits generation of higher resolution features on the target surface [21]. The substrate used was Fisher brand Microscope Cover Glass (12-545-102 from Fisher Scientific, circles of 25 mm in diameter and 0.15 ± 0.02 mm thick). Laser-micromachined patterns were determined by computer programming and stage motion control was achieved by the company-supplied program interface (Resonetics Process Controller). Key parameters, such as fluence, pulse number and repetition rate, were varied. Micro-machined samples were coated with gold by sputter coating, and examined under Scanning Electron Microscope (SEM). The acquired SEM images were analyzed by ImageJ software [22].

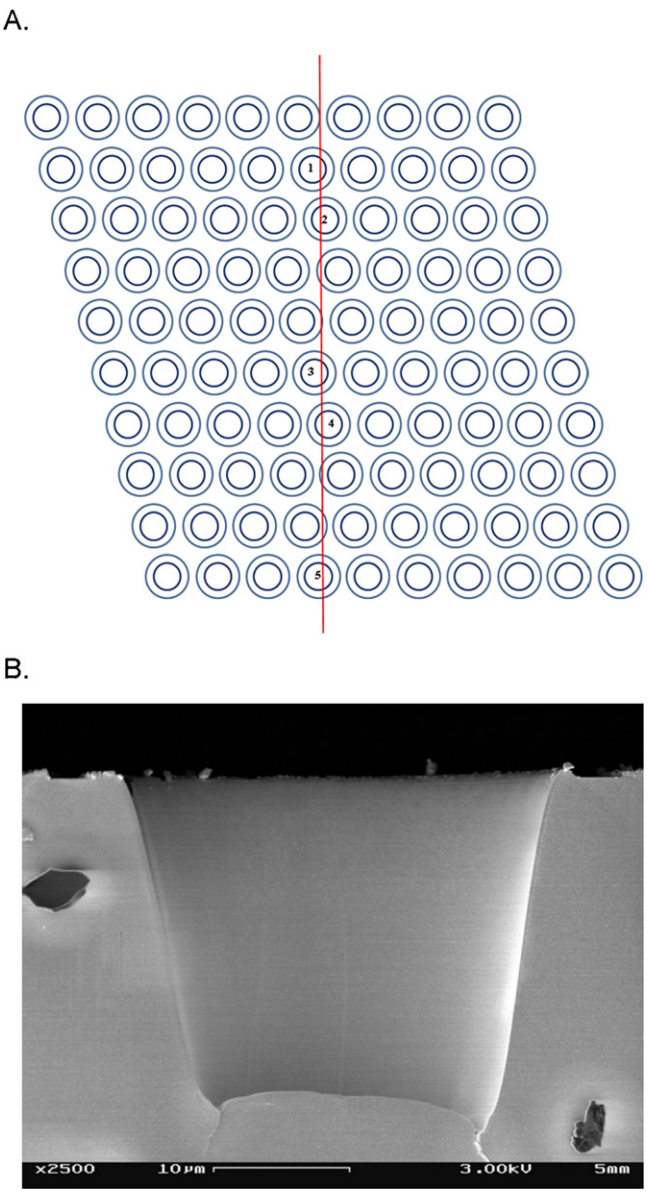

Fig. 1. (A) Schematic topview of the microwell-structured surface. The vertical line represents the cut to reveal vertical well sections. Circles represent top and base of each microwell; (B) Cross-section view of a typical microwell fabricated at a fluence of 1.0 J/cm^2, pulse number of 212; repetition rate of 100 Hz.

2.2. Cell culture and time-lapse microscopy

Plane glass cover slips were used as the control substrate. Before use, sample and control cover slips were cleaned by ultrasonication in D.I. water for 10 min and then sterilized with UV lighting for no less than 30 min. After drying in air at room temperature, the cover slips were treated with 0.2% gelatin (Sigma–Aldrich, MO) solution in D.I. water in a sterile hood for 1 h and aerated for 20 min after removing the solution, followed by washing twice with PBS prior to use.

Human fibroblast cells (SCRC-1041 from ATCC) were cultured in growth medium containing 15% fetal bovine serum (Summit, CO) and 85% Dulbecco's modified Eagle's medium (DMEM) (ATCC, VA) with 4 mM L-glutamine, adjusted to contain 1.5 g/L sodium bicarbonate and 4.5 g/L glucose. The culture medium was changed every two days until cells reached confluence. Confluent cells were trypsinized and resuspended according to ATCC protocol, followed by uniform seeding on gelatin-coated glass substrates. Cells were

Table 1
Effect of cumulative dose on fabricated microwell depth[a].

Laser fluence (J/cm^2)	Pulse number	Cumulative dose (J/cm^2)	Microwell depth (μm)[b]	Microwell depth/Cumulative dose (μm/(J/cm^2))
7.10	212	212.0	19.93	0.0940
10.65	212	318.0	30.02	0.0944
14.20	212	424.0	40.00	0.0943
17.55	212	530.0	48.58	0.0917

[a] Laser frequency was 100 Hz.
[b] Values are averages of at least 3 measurements – standard deviations were all less than 2%.

incubated in WaferGen SHZ00 system (WaferGen Biosystems, CA) and phase contrast imaging was performed overnight for 8 h on the Nikon Eclipse TE2000-S Microscope. Images were collected every min, using a 10× objective. Acquired images were processed and analyzed by Image-Pro Plus and ImageJ software. Unless otherwise stated, the data presented is representative of at least three independent replications.

3. Results

3.1. Microstructure architecture and process optimization

The ArF excimer laser illuminates a mask which works at 20× demagnification for the image with a lens of 75 mm focal length. With focus and aperture finely adjusted to optimal settings, this imaging arrangement produces relatively sharp edges in the ablation process. By simply changing masks with different sizes, we were able to fabricate microwells ranging in diameter from 5 μm to 100 μm without varying the energy density per pulse (fluence), delivered to the sample surface, and thereby maintain constant ablation conditions. Fluences ranging from 1.0 to 2.5 J/cm^2 were applied.

To examine the cross-section features of the fabricated microwells, a 10 × 10 matrix of identical microwells, as illustrated in Fig. 1A, was produced with each row shifted to the right by 1/10 of the microwell size. A diamond glass cutter was used to cut the matrix in half in the vertical direction from the back to reveal cross-section features for direct depth measurement. Owing to the high precision of laser micromachining techniques, all fabricated microwell dimensions were measured to have an error less than 2%.

Other conditions being equal, each laser pulse resulted in essentially the same material removal from the target site. Fig. 1B shows an example of cross-section view of fabricated microwells and Fig. 2 shows the highly linear (R^2 = 0.9971) relationship of microwell depth up to 50.08 μm with pulse number up to 526. The rate of material removal at a fluence level of 1.0 J/cm^2 came to 0.094 μm/pulse. Cracks around the base edges, evident in Fig. 1B were observed, probably due to material shrinkage upon cooling. The depth of the ablated microstructure can be predicted by introducing a combined parameter, cumulative dose, which is defined as the product of laser fluence and pulse number. As shown in Table 1, the division of fabricated microwell depth by the cumulative dose is a constant for glass.

Although the shape of the image at the target surface resembles the true shape of the mask, during near-field imaging, the perimeters of the product tended to decrease with depth, into the material, which is an intrinsic feature quite different from a conventional

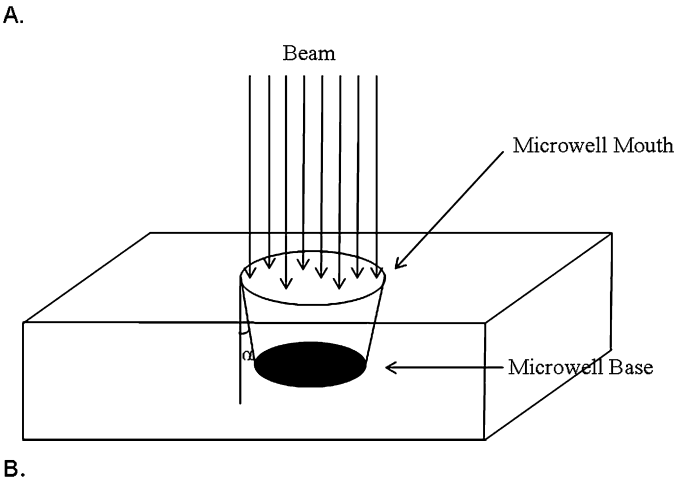

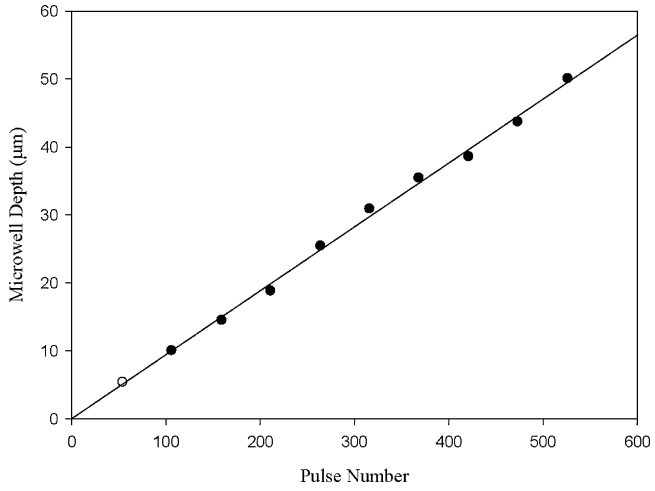

Fig. 2. Plot of microwell depth (μm) vs. pulse number at a fluence of 1.0 J/cm^2 and repetition rate of 100 Hz.

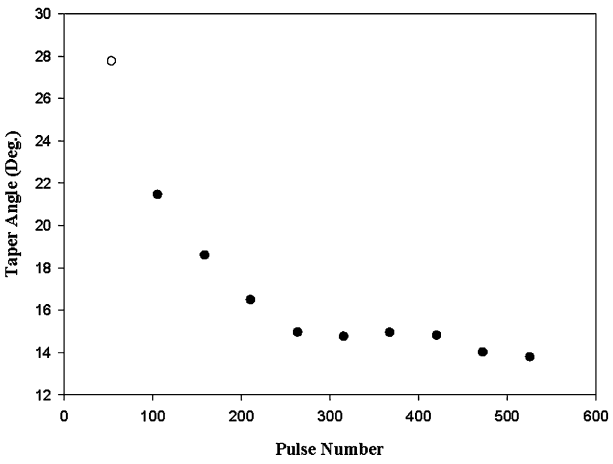

Fig. 3. (A) Schematic representation of taper effects by laser micromachining onto the substrate (α is the taper angle); (B) Plot of taper angle vs. pulse number at a fluence of 1.0 J/cm^2 and repetition rate of 100 Hz.

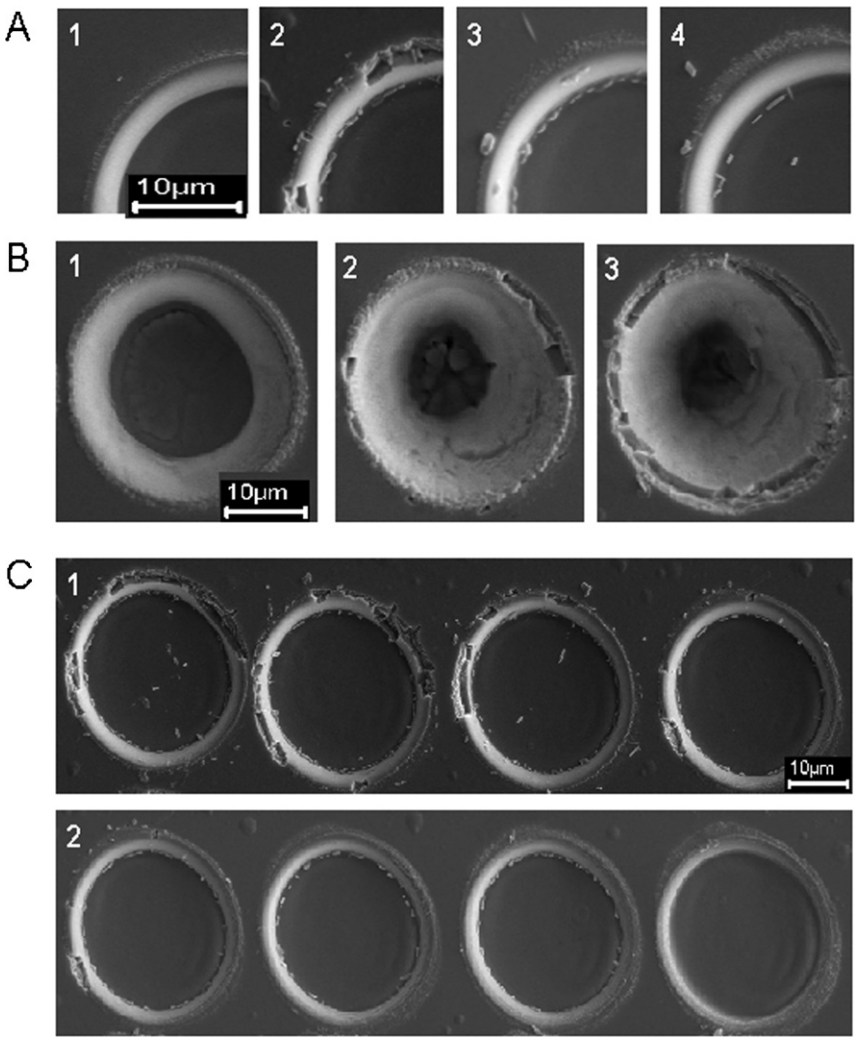

Fig. 4. Edge effects in terms of fluence, pulse number and repetition rate. (A) Zoom-in comparisons of first circle quarters. Pulse number of 53; repetition rate of 10 Hz, fluence (J/cm^2) of (1) 1.0; (2) 1.2; (3) 1.5; (4) 2.0. (B) Fluence (J/cm^2) of 1.0; repetition rates of 60 Hz; pulse number of (1) 159; (2) 318; (3) 477. (C) Fluence (J/cm^2) of 1.2; pulse number of 53; from left to right, repetition rates (Hz) of (1) 10, 60, 110, 160; (2) 160, 210, 260, 310.

mechanical drill [21]. As shown in Fig. 3A, we defined the taper angle between the walls of the measured microwell and the vertical line as α. The taper angle (α) can be reduced by using high fluence, increasing irradiation, switching to different objective lenses or a double-sided drilling. Fig. 3B shows the relationship between α and the pulse number. The taper angle tended to decrease as the pulse number increased owing to the removal of residual wall material with increased UV radiation. Table 2 illustrates how α was reduced as a function of laser fluence.

As the microwell deepens, a visible deposit develops on the surrounding sample surface and form fringes, which migrate outwards as the deposit thickens nearer the ablation site. Also, laser energy absorption causes melting, which results in a thin layer of material on the interior walls as well as on the microwell opening edges. If the deposition of vapor after ambient cooling cannot cover the initial superficial cracks, which usually occur around the microwell opening edges, permanent chips and debris form. In this study, N_2 was used as the processing gas to reduce debris formation. At a laser fluence of 1.2 J/cm^2, chipping was prevalent. As shown in Fig. 4A(2), cracking extensively occurred and chips were found all along the microwell opening edges, even when low laser irradiation (pulse number) was applied. At either higher or lower fluence levels, no obvious breaking effects were observed; however, evident melting effects were seen at higher fluence levels. In terms of pulse number, however, both breaking and melting effects were promoted as pulse number increased (Fig. 4B). For example, no breaking effects were observed in Fig. 4B(1), while in Fig. 4B(2), breaking effects occurred. In Fig. 4B(3), however, chipping became predominant. As illustrated in Fig. 4C, chipping was eliminated by increasing the repetition rate to promote melting; even at the laser fluence of 1.2 J/cm^2, with which chipping at edges was prevalent. A trial-and-error approach yielded conditions for fabricating microwells on glass by laser micro-machining that eliminated chipping. These conditions were laser fluence of 1.0 J/cm^2, repetition rate of 100 Hz, and pulse number calculated by dividing the desired microwell depth (μm) by 0.094 (μm).

Table 2
Effect of laser fluence on taper angle[a].

Fluence (J/cm^2)	Taper angle (°)
7.10	18.60 ± 7.08 (n = 7)
10.65	11.36 ± 5.33 (n = 7)
14.20	10.50 ± 1.63 (n = 7)
17.55	9.03 ± 2.15 (n = 7)

[a] Total number of applied pulses was 159 with a frequency of 100 Hz.

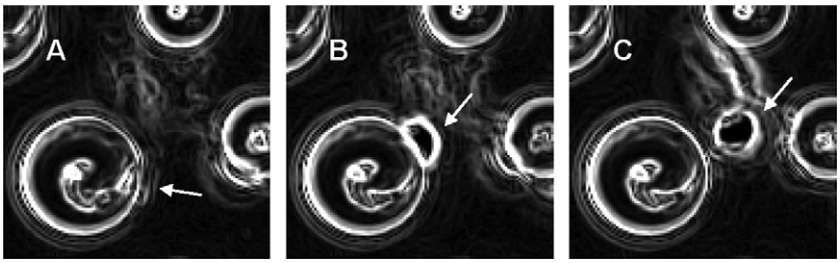

Fig. 5. Sample cell "climbing" out of microwells after initially falling in. Time-lapse microscopy images were taken at different times: (A) 114 min; (B) 119 min; (C) 128 min. The lamellipodia is indicated by the arrow. A total of 67 cells from 83% of microwells in view (data pooled from three separate observations) exhibited this behavior. (In order to make cell shape more discernable, original images were processed by the "edge finding" function of ImageJ).

3.2. Cell-microwell interactions

Microwells, 20 μm deep, were micromachined in six replicates to create a 6 × 10 array. The size of the array was chosen to fit into the time-lapse microscope view with a 10× objective. The human fibroblast cells used in this study exhibit a relatively uniform cell size of 26.24 ± 4.74 μm in suspension. After initial adhesion within the first several hours, cells were multiple times larger than their initial sizes due to flattening. Preliminary cell culture studies had revealed that microstructured surfaces with certain microwell sizes did not support cell adhesion and growth, even when the microwell sizes were larger than the suspended cell size – the structures seemed to repel cells (data not shown). The purpose of time-lapse studies was to observe the cell-structure interaction in the first few hours of seeding to provide a better understanding or explanation of the repulsive potential of microstructures surfaces hypothesized from the preliminary work.

Time-lapse studies revealed that cells did not fall into microwells of equal or lower than 30 μm in diameter, probably due to the cell size matching or being smaller that the microwell openings. Cells successfully fell in larger microwells, but tended to "climb" out soon after. Fig. 5 shows a typical example. A cell from a 40 μm microwell (Fig. 5A) sensed the flat surface with lamellipodia at 114 min and was partly out of the well within 5 min (see Fig. 5B). Nine minutes later, the whole cell body was out of the microwell and got situated between two neighboring microwells (Fig. 5C). This type of behavior was observed from approximately 83% of the microwells in view (data pooled from three replicates) with at least one cell (total of 67 cells). Of the 67 cells, 51 crawled out and settled on the flat surface outside the wells within 3 h of plating. The remaining cells either detached and floated away, or showed signs of loosing viability. It is interesting to note that Khademhosseini et al. [23] had to fabricate microwells as large as 200 μm in diameter and 120 μm deep to contain cells, attesting to the well-size dependence of the above reported behavior.

Accurately tracking cell movement is not straightforward as cells change shape and size as they migrate on the substrate. This issue must be dealt with whether cell tracking is conducted automatically or manually by computer software [24,25]. Changes in cells' morphology from frame to frame can make it difficult for software to effectively identify the same cell over frames and also determine the exact location of the center of the cell [26]. Manual tracking was selected in this study as it resulted in cell tracks that represented the actual path of the cells more accurately. Cells that remained stationary, or moved outside the viewing area, or that underwent cell division during the course of observation were excluded from the tracking procedure.

Fig. 6A–E illustrates five typical trajectories when cells approached nearby microwells and Fig. 6F–H illustrates three typical trajectories of cells that "climbed" out of microwells and maintained motion on the surrounding surface. Cells were tracked over the first 3 h after seeding, and their coordinates were recorded every 2 min. Cells were seen falling in large microwells. However, when a cell approached a microwell with a comparable size of the cell, it tended to move away instead of moving in. When the cell started out on flat surface, a "random walk" occurred as expected.

The method employed to determine the direction relative to near-by microwell at each frame (time point) is illustrated in Fig. 7. Locations 1, 2 and 3 are successive frame positions. Outward direction of cell movement is defined if $\gamma \geq 90^\circ$ and inward direction is defined if $\gamma < 90^\circ$. The results presented in Table 3 were generated from a total of 24 cells and show that the probability of cell outward movement increased as the distance between the cell and the microwell edge decreased to 6 μm. The closer the cell got to a microwell, the more significant the repulsion came into play. Cell velocity was measured to be 54.01 ± 15.53 μm/h on flat surface, which is consistent with published values [26,27] in absence of contact inhibition. Under the influence of microstructure, however, cells moved at significantly faster speeds (Table 3). However, no significant cell speed difference was observed for different cell-to-well distances (Table 3).

3.3. Cell spreading on microstructured surfaces with microwells smaller than or equal to 30 μm

After seeding, initial cell adhesion on glass occurred in the first hour, and lamellipodia formation was observed, followed by complete spreading. Fig. 8 shows a typical interaction with 20 μm microwells. When the lamellipodia wave front encountered a microwell, cell spreading was divided onto non-well flat surface. As shown in Fig. 8A (arrow a), the well-spread cell projected its lamellipodia evenly. However, when it got closer to the microwell, the wave front at the microwell edge retracted (Fig. 8B, arrow c) and spreading continued on the flat surface in between the microwells (Fig. 8C, arrow d). When a microwell was encountered sideways of the major spreading direction, the cell tended to attach along the edges of the well instead of either getting in or bridging it (Fig. 8A, arrow b)

On more compact arrays (less space between microarrays), cell shape on the micro-structure was largely confined by neighboring microwells. Cells on these microwell structures were on the move to "get away" from this spatial constraint. The example provided in Fig. 9, is an excellent illustration due to the fact that it occurred at the edge of the microwell structuring. The cell identified after 274 min (Fig. 9A, arrow) had been on the move onto the flat surface in between well for some time. At 308 min (Fig. 9B), cell membrane lamellipodia sensed the large flat surface and at 388 min (Fig. 9C), large lamellipodia developed onto the flat surface. In Fig. 9D and E, the cell was completely away from the microstructured surface and had settled on the flat surface as suggested by noticeable lamellipodia retractions. Similarly the cell did not turn around back in contact with the microwells. This behavior was observed in a total of 31 cells that fell at the edge of the microwell pattern.

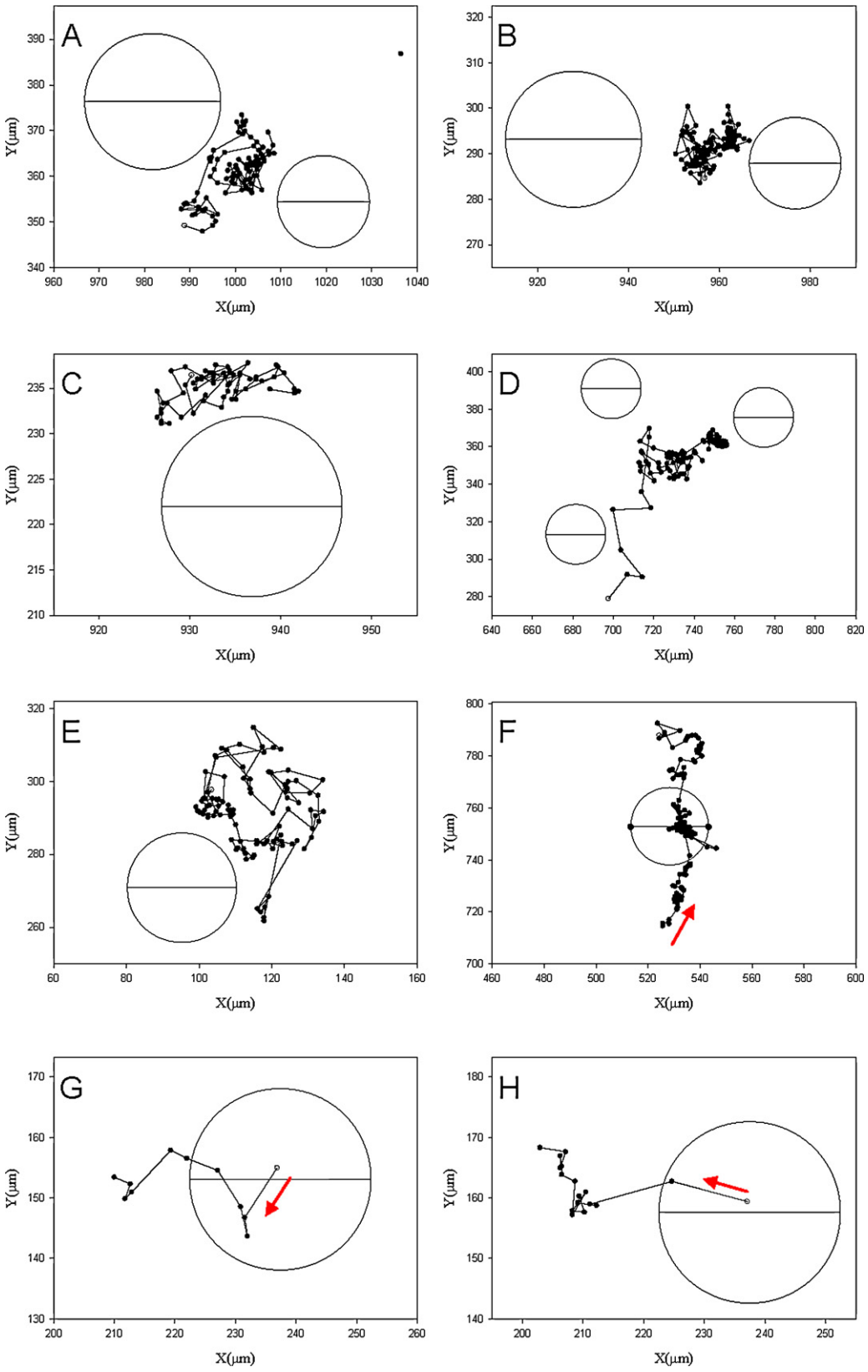

Fig. 6. Samples of cell locomotion trajectories on microstructured glass (with microwells) within the first 3 h after cell seeding. (A–E) Five typical trajectories in close proximity to nearby microwells. (F–H) Three typical trajectories from cells that were initially inside a microwell.

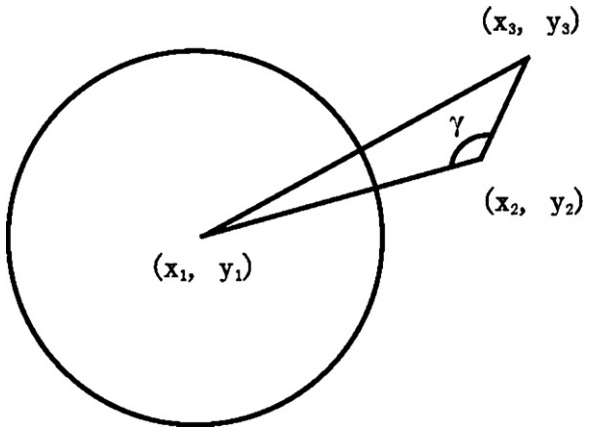

Fig. 7. Schematic illustration of trajectory analysis employed to determine the direction relative to in-contact microwell at each frame (time point). Outward direction of cell movement is defined if $\gamma \geq 90^{\circ}$ and inward direction is defined if $\gamma < 90^{\circ}$.

Table 3
Probability of cell outward movement as a function of distance between cell center and microwell edge.

Cell-to-well distance (μm)	Probability of outward movement[a] (%)	Cell movement velocity (μm/h)
20	48	79.34
18	47	80.23
16	48	78.62
15	49	77.13
14	51	77.62
13	51	76.73
12	52	77.77
11	55	75.88
10	56	75.77
9	54	76.98
8	55	75.29
7	54	72.18
6	57	67.79
5	65	69.98
4	75	77.29
3	83	73.70

[a] The probability was calculated by dividing the number of outward movements by all movements from a total of 24 cells at approximately the same well-to-cell distance from images such as those presented in Fig. 6.

4. Discussion

Cell migration paths are dictated by both the migration speed and the time period over which the cell front continues in roughly the same direction (directional persistence) [28,29]. These defining parameters are governed by biophysical events such as forward protrusion of lamellipodia, formation of new attachments to substratum, generation of contractile forces to translocate the cell body, and rear detachment from the substratum [30]. Cells exhibited faster migration speed on the microstructure (75.77 ± 3.36 μm/h) than on flat surfaces (54.01 ± 15.53 μm/h), attributable to weaker cell adhesion. It is generally accepted that firm cell adhesion hinders cell migration [31]. A separate study in our laboratory, to be published separately, has confirmed this explanation.

Time-lapse results revealed that cells that fell into microwells on seeding "climbed" out of the microwells. Once cells "climbed" out of the microwells, they avoided getting into neighboring microwells. Also, cells that started out on the flat surfaces in between the microwells, in a similar way not only avoided getting into neighboring wells, but also tended to move away once they sensed a nearby microwells, while on flat surface, random movement occurs as long as there was no contact inhibition of cell movement. These time-lapse findings confirmed the microstructured repulsion effect

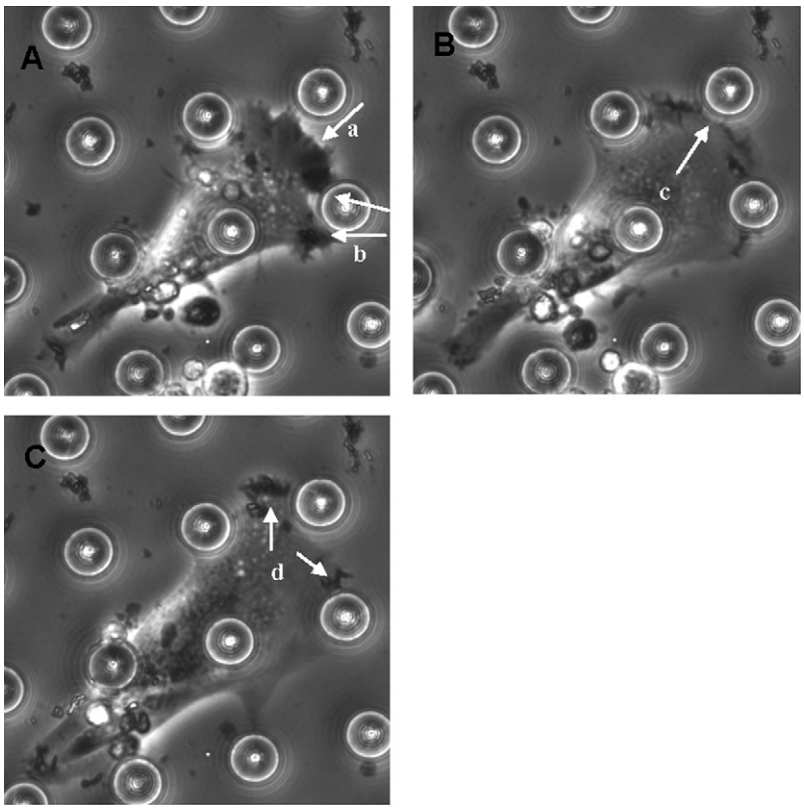

Fig. 8. Cell spreading on microwell-structured glass surface (microwell size: 20 μm, spacing between neighboring microwell edges: 30 μm). Time-lapse microscopy images were taken at different times: (A) 6 h; (B) 7 h; (C) 10 h.

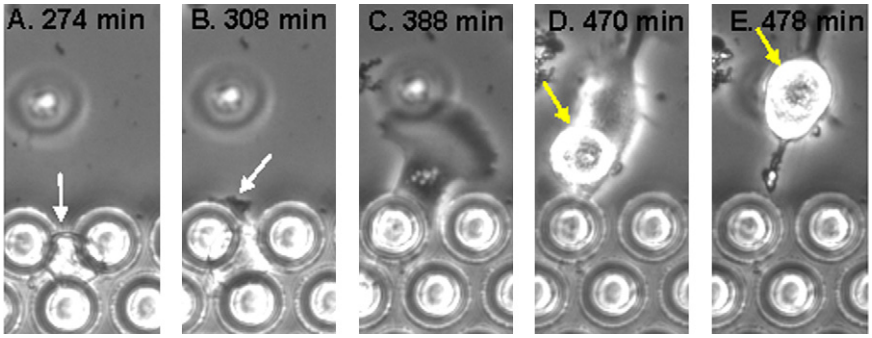

Fig. 9. Cell locomotion on contact microwell-structured glass surface (microwell size: 30 μm, spacing between neighboring microwell edges: 5 μm). (A) 274 min; (B) 308 min; (C) 388 min; (D) 470 min; (E) 478 min. The yellow arrow in D and E identifies a dead cell on top of the cell of interest (For interpretation of the references to color in this figure legend, the reader is referred to the web version of the article).

hypothesized from our preliminary results, where few or no cells were found on microstructured substrates in long term (days) cultures – cells that ended up on microstructured surfaces were not dying, instead they moved (or were repelled) away from the microstructured glass surfaces.

The question that begs an answer is what is the mechanism of microstructured surface-fibroblast cell repulsion? Glass is a widely used substrate material that is well known for its chemical and thermal inertness. In a slightly different system, Dd:YAF laser and bioglass – whose major constituent (SiO_2) is similar to that of borosilicate glass, there was practically no change in glass chemical composition [32], suggesting that this is probably the case with ArF laser micromachining as well. This suggests a chemical based repulsion unlikely. It is possible that the orientation of the cells on microstructured surfaces influence cell responses, much like in the so-called "contact guidance." Cells are well known to orient themselves along the micro-features they get in contact with [33–35]. While this, together with spatial restriction, may explain the difference in locomotion speed, it still does not explain the change in direction when approaching a microwell structure. Probably when lamellipodia senses the curvature or wall slope, signals similar to standard chemical repulsion signals are generated that eventually prescribe the observed cell behavior. More detailed studies are needed to better understand the observations in this study.

As reported by Nikkhah et al. [36], fibroblastic cells adhered well to rigid substrates with abundant parallel and cross-link formation of actin filaments. Typically, highly organized cytoskeleton within the cells is developed and a state of high tension is produced by formation of stress fibers, lamellipodia, and focal adhesions. Cell shape stability in stretching and avoiding growing along sidewalls is determined by the balance between cytoskeletal pre-stress and the mechanical force within the cell body [37]. A study of the cytoskeleton dynamics for cells on microstructured surfaces in parallel with standard chemical repulsion experiments is likely to provide insights into the signaling involved.

Although further mechanism studies with glass and fibroblasts are needed, it is reasonable to propose expanding theses studies to other more practical (implantable) materials, with the goal of establishing in vitro proof-of-concept of microtstructuring in elongating the lifespan of in vivo biosensors and medical implants.

5. Conclusions

A cell-surface interaction study with human fibroblasts on glass, microstructured with microwells, was carried out several hours after seeding. The results support the following conclusions: (1) High-aspect-ratio microwells fabricated in glass, endow the resulting structures with human fibroblast repulsion properties, through a mechanism that is not yet well understood. (2) Human fibroblast cells moved on microwell structured glass surfaces at significantly higher speeds in comparison to control glass surfaces.

Acknowledgements

We thank Ms. Yinzhi Lai and Ms. Lina Wang for their technical assistance. This study was supported by NSF (ECS-0304340) and UGA engineering grants.

References

[1] N. Wisniewski, M. Reichert, Methods for reducing biosensor membrane biofouling, Colloids and Surfaces B: Biointerfaces 18 (2000) 197–219.
[2] D.G. Castner, B.D. Ratner, Biomedical surface science: foundations to frontiers, Surface Science 500 (2002) 28–60.
[3] T.I. Croll, A.J. O'Connor, G.W. Stevens, J.J. Cooper-White, Ablankslate layer-by-layer deposition of hyaluronic acid and chitosan onto various surfaces, Biomacromolecules 7 (2006) 1610–1622.
[4] Y. Liu, S. Sun, S. Singha, M.R. Cho, R.J. Gordon, 3D femtosecond laser patterning of collagen for directed cell attachment, Biomaterials 26 (2005) 4597–4605.
[5] A.S. Andersson, F. Backhed, E.A. von, A. Richter-Dahlfors, D. Sutherland, B. Kasemo, Nanoscale features influence epithelial cell morphology and cytokine production, Biomaterials 24 (2003) 3427–3436.
[6] C.H. Choi, S.H. Hagvall, B.M. Wu, J.C. Dunn, R.E. Beygui, C.J. Kim, Cell interaction with three-dimensional sharp-tip nanotopography, Biomaterials 28 (2007) 1672–1679.
[7] E.K.F. Yim, R.M. Reano, S.W. Pang, A.F. Yee, C.S. Chen, K.W. Leong, Nanopattern-induced changes in morphology and motility of smooth muscle cells, Biomaterials 26 (2005) 5405–5413.
[8] D. Khang, J. Lu, C. Yao, K.M. Haberstroh, T.J. Webster, The role of nanometer and sub-micron surface features on vascular and bone cell adhesion on titanium, Biomaterials 29 (2008) 970–983.
[9] S.D. Fewster, R.R.H. Coombs, J. Kitson, S. Zhou, Precise ultrafine surface texturing of implant materials to improve cellular adhesion and biocompatibility, Nanobiology 3 (1994) 201–210.
[10] A.M. Green, J.A. Jansen, D.W.J.P. Van, R.A.F. Von, Fibroblast response to microtextured silicone surfaces: texture orientation into or out of the surface, Journal of Biomedical Materials Research 28 (5) (1994) 647–653.
[11] C.E. Campbell, R.A.F. Von, Microtopography and soft tissue response, Journal of Investigative Surgery 2 (1) (1989) 51–74.
[12] M. Nematollahi, D.W. Hamilton, N.J. Jaeger, D.M. Brunette, Hexagonal micron scale pillars influence epithelial cell adhesion, morphology, proliferation, migration, and cytoskeletal arrangement, Journal of Biomedical Materials Research Part A 91 (1) (2009) 149–157.
[13] T.C. Chang, P.A. Malian, Excimer pulsed laser ablation of polymers in air and liquids for micromachining applications, Journal of Manufacturing Processes 1 (1) (1999) 1–17.
[14] Y. Chen, K. Naessens, R. Baets, Y. Liao, A.A. Tseng, Ablation of transparent materials using excimer lasers for photonic applications, Optical Review 12 (6) (2005) 427–441.
[15] K. Nakata, M. Umehara, T. Tsumura, Excimer laser ablation of sintered hydroxyapatite, Surface and Coatings Technology 201 (9–11) (2007) 4943–4947.
[16] A.A. Tseng, Y. Chen, K. Ma, Fabrication of high-aspect-ratio microstructures using excimer laser, Optics and Lasers in Engineering 41 (6) (2004) 827–847.
[17] D. Figeys, D. Pinto, Lab-on-a-Chip. A revolution in biological and medical sciences, Analytical Chemistry 72 (9) (2000) 330–335.
[18] S.M. Pegrum, N.G. Maroudas, Early events in fibroblast adhesion to glass: an electron microscopic study, Experimental Cell Research 96 (2) (1975) 416–422.
[19] J. Desbiens, P. Masson, ArF excimer laser micromachining of Pyrex. SiC and PZT for rapid prototyping of MEMS components, Sensors and Actuators A Physical 136 (2) (2007) 554–563.

[20] E. Gottwald, S. Giselbrecht, C. Augspurger, B. Lahni, N. Dambrowsky, R. Truckenmüller, V. Piotter, T. Gietzelt, O. Wendt, W. Pfleging, A. Welle, A. Rolletschek, A.M. Wobus, K.F. Weibezahn, A chip-based platform for the in vitro generation of tissues in three-dimensional organization, Lab on a Chip 7 (2007) 777–785.
[21] D. Palanker, S. Ohad, A. Lewis, A. Simon, J. Shenkar, S. Penchas, N. Laufer, Technique for cellular microsurgery using the 193 nm excimer laser, Lasers in Surgery and Medicine 11 (1991) 580–586.
[22] M.D. Abramoff, P.J. Magelhaes, S.J. Ram, Image processing with ImageJ, Biophotonics International 11 (7) (2004) 36–42.
[23] A. Khademhosseini, L. Ferreira, J. Blumling, J. Yeh, J.M. Karp, J. Fukuda, R. Langer, Co-culture of human embryonic stem cells with murine embryonic fibroblasts on microwell-patterned substrates, Biomaterials 27 (2006) 5968–5977.
[24] M. Bindschadler, J.L. McGrath, Sheet migration by wounded monolayers as an emergent property of single-cell dynamics, Journal of Cell Science 120 (5) (2007) 876–884.
[25] C. Decaestecker, O. Debeir, P. VanHam, R. Kiss, Can anti-migratory drugs be screened in vitro? A review of 2D and 3D assays for the quantitative analysis of cell migration, Medicinal Research Reviews 27 (2) (2007) 149–176.
[26] A. Tremel, A. Cai, N. Tirtaatmadja, B.D. Hughes, G.W. Stevens, K.A. Landman, A.J. O'Connor, Cell migration and proliferation during monolayer formation and wound healing, Chemical Engineering Science 64 (2009) 247–253.
[27] P.K. Maini, D.L.S. McElwain, D. Leavesley, Travelling waves in a wound healing assay, Applied Mathematics Letters 17 (2004) 575–580.
[28] M.H. Gail, C.W. Boone, The locomotion of mouse fibroblasts in tissue culture, Biophysical Journal 10 (1970) 980–993.
[29] G.A. Dunn, Characterising a kinesis response: time averaged measures of cell speed and directional persistence, Agents and Actions [Suppl.] 12 (1983) 14–33.
[30] D.A. Lauffenburger, A.F. Horwitz, Cell migration: a physically integrated molecular process, Cell 84 (1996) 359–369.
[31] A. Misra, R.P.Z. Lim, Z. Wu, N-WASP plays a critical role in fibroblast adhesion and spreading, Biochemical and Biophysical Research Communications 364 (2007) 908–912.
[32] L. D'Alessio, R. Teghil, M. Zaccagnino, I. Zaccardo, D. Ferro, V. Marotta, Pulsed laser ablation and deposition of bioactive glass as coating material for biomedical applications, Applied Surface Science 138–139 (1999) 527–532.
[33] Y. Wan, Y. Wang, Z. Liu, X. Qu, B. Han, J. Bei, S. Wang, Adhesion and proliferation of OCT-1 osteoblast-like cells on micro- and nano-scale topography structured poly(L-lactide), Biomaterials 26 (2005) 4453–4459.
[34] D.M. Brunette, Fibroblasts on micromachined substrata orient hierarchically to grooves of different dimensions, Experimental Cell Research 164 (1986) 11–26.
[35] P.T. Ohara, R.C. Buck, Contact guidance in vitro. A light transmission and scanning electron microscopic study, Experimental Cell Research 121 (1979) 235–249.
[36] M. Nikkhah, J.S. Strobl, B. Peddi, M. Agah, Cytoskeletal role in differential adhesion patterns of normal fibroblasts and breast cancer cells inside silicon microenvironments, Biomedical Microdevices 11 (2009) 585–595.
[37] D.E. Ingber, I.I. Tensegrity, How structural networks influence cellular information processing networks, Journal of Cell Science 116 (2003) 1397–1408.